Rocking incremental dynamic analysis

Article *in* Earthquake Engineering & Structural Dynamics · December 2021

DOI: 10.1002/eqe.3586

CITATION
1

READS
386

2 authors:

Christos Lachanas
National Technical University of Athens
8 PUBLICATIONS **6** CITATIONS
SEE PROFILE

Dimitrios Vamvatsikos
National Technical University of Athens
200 PUBLICATIONS **7,777** CITATIONS
SEE PROFILE

Rocking incremental dynamic analysis

C. G. Lachanas,[1*] D. Vamvatsikos[1]

[1] *School of Civil Engineering, National Technical University of Athens, Athens, Greece.*

Summary

The seismic response assessment of rocking systems via Incremental Dynamic Analysis (IDA) is investigated, focusing on the issues that arise in the analysis and postprocessing stages. Rocking IDA curves generally differ from those of hysteretic structural systems due to (i) the frequent appearance of resurrections, (ii) their highly weaving non-monotonic behavior, and (iii) their overall high variability. Hence, including or ignoring analysis results above the first resurrection level, deriving statistics given a response level versus an intensity measure level, as well as selecting an adequate number of ground motion records and runs per record, become challenging issues with non-trivial impact on the probabilistic characterization of rocking response. This necessitates a fresh view on analysis choices and post-processing techniques, aiming to assure the accuracy and fidelity of rocking IDA results. As an example, the effect of different choices and techniques are showcased on two-dimensional rigid blocks that are assumed to represent simplified models of monolithic ancient columns of different slenderness.

KEYWORDS

incremental dynamic analysis, rigid rocking blocks, seismic demands, response statistics

1 INTRODUCTION

Assessing the rocking response of freestanding rigid blocks via Incremental Dynamic Analysis (IDA, [1, 2]) is the focus of our work. Numerous ancient monuments comprise rigid unanchored blocks and columns that undergo rocking response during an earthquake. Contemporary literature and practice abound with concepts on employing rocking as a seismic protection mechanism for bridge piers [e.g., 3], walls [e.g., 4] or pedestal structures [e.g., 5]. Starting from Housner in 1963 [6] who proposed the equation of motion for a rigid rocking block (Figure 1a), numerous studies [7–18] have investigated the effect of block and ground motion characteristics on the full range of rocking response. Others have assessed the response of rocking non-structural components [19–20], while testing campaigns [19, 21] have explored the validity of analytical solutions. In other words, focusing on rocking is self-explanatory; staying with IDA may not be as simple to explain apart from a certain affinity of the second author.

IDA is a method for assessing the performance of structures via nonlinear response history analysis. Based on the gradual scaling of a single suite of ground motions, it covers the full behavior range of a structural system, from the non-damaging response at low intensity levels, to its failure (local or global collapse) at the higher ones. The results appear as continuous IDA curves of intensity measure (IM) versus engineering demand parameter (EDP) values. It has served as a computational tool for numerous studies and guidelines regarding the seismic response, as well as the vulnerability and loss assessment of engineering structures [e.g., 22–24]. It does not stand alone in this field, as alternative assessment methods are available in the literature, each representing a different way of running and postprocessing nonlinear response history analyses. Multi Stripe Analysis (MSA) [25] employs one or more suites of records at given levels of intensity, forming characteristic stripes of results in the IM-EDP plane. In Cloud Analysis [26], one or more uniformly scaled or fully unscaled suites of ground motions are used to conduct the assessment, appearing as distinct IM-EDP clouds.

While at their inception all three methods could be said to be competing neck to neck, the game changer was the introduction of record selection [27–30]. This high-end technique introduces site-specific hazard consistency to the ground motion set employed for analysis, imparting increased fidelity to the assessment results. As hazard consistency typically needs to be addressed anew at each IM level, MSA (primarily) and multiple Cloud Analysis (secondarily) can better take advantage of record selection. IDA, by virtue of using a single record suite at all intensity levels is disadvantaged. Still, optimal selection at a single high-intensity level or a combination of multiple levels can enforce at least partial hazard consistency [30] where it matters. Coupled with highly efficient intensity measures [31–34], it can be argued that IDA remains relevant in its third decade of life, offering a simple approach for comprehensive probabilistic treatment of seismic performance.

[*] Corresponding author: lahanasch@central.ntua.gr

Nevertheless, rocking systems present new challenges to the application of all pertinent approaches and IDA in particular. For example, even before Vamvatsikos and Cornell [1], Psycharis et al. [35] showed the difficulty in capturing the seismic response of multi-drum ancient columns under scaled ground motions. Figure 1b captures a typical rocking IDA curve of a rigid rectangular block for an ordinary (no-pulse-like, no-long-duration) record following Housner's simplified model [6]. The scaling of the record was made on a constant step of 0.01 g for the IM, herein the Peak Ground Acceleration (*PGA*), while the peak rocking angle normalized by the block slenderness, $\tilde{\theta} = \theta_{max}/\alpha$, was employed as the EDP. As shown, the high nonlinearity of the rocking motion results into weaving [1] behavior of the IDA curve, while instances of overturning collapse at a given IM level followed by non-overturning behavior at a higher IM, so-called "resurrections" [1], are a relatively frequent phenomenon. This behavior is atypical for hysteretic IDAs and nearly always discounted [1, 2]; for rocking it is the norm, and it bears consequences. Actually, it is noted from the very start that employing a spline fit of individual IM-EDP points per Vamvatsikos and Cornell [2] becomes a dangerous proposition for rocking IDA curves. Given the weaving behavior, splines may prove to be too rigid to fit the rapidly changing curves, leading to biased results. Therefore, in all discussions to follow, a piecewise linear fit is universally applied to span discrete points. This is also the general recommendation for all practical purposes, unless one is prepared to expend hundreds or thousands of response history analyses.

Such findings indicate that the analysis choices and the post-processing techniques for IDA need to be revisited for the case of rocking blocks to ensure the fidelity and efficiency of the results. Aiming to provide such an outlook, the issues that arise when employing IDA to rocking blocks are presented and discussed in detail, offering efficient techniques for post-processing the results of nonlinear response history analyses to achieve reliable probabilistic characterization. Although all examples presented pertain to planar rocking blocks, the techniques and approaches discussed are general and deemed to be applicable to all rocking systems, or furthermore to all systems with highly weaving behavior and/or encumbered by resurrections.

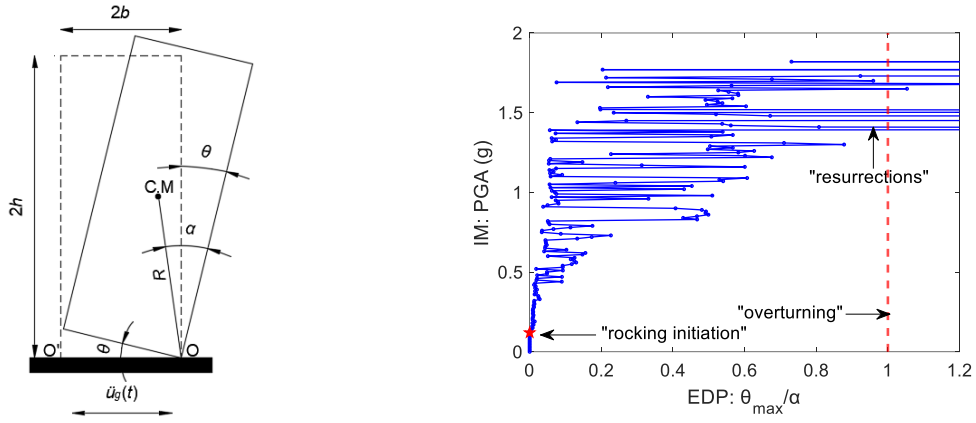

(a) (b)

Figure 1. a) Planar rocking block on a rigid base. b) Typical IDA curve of a rocking block for a single ground motion.

2 IDA RUNNING AND POST-PROCESSING OPTIONS

Herein, we present the issues that differentiate the application of IDA to rocking systems versus hysteretic ones, focusing on techniques to overcome them. All example results shown are taken from the analysis of a typical rectangular rigid block with base width (2*b*) of 1.33 m and height (2*h*) of 12.00 m using ordinary ground motions and following the idealization of Housner [6].

2.1 To resurrect or not to resurrect?

There is nothing unnatural with a structural system exceeding its global collapse capacity at a given IM level, while surviving the same excitation at higher scaling. This behavior has been observed in several occasions in the literature, and it gained visibility in the context of IDA as an uncommon occurrence for some hysteretic systems. In such cases, the rare appearances of structural resurrection are heavily dependent on the details of the model and analysis approach and they typically only slightly precede the appearance of a final no-return flatline, making it natural (and algorithmically simpler) to discard any stable response at IMs higher than the first sign of dynamic

instability. Neglecting resurrection becomes a whole different proposition when rocking response is investigated via IDA, since multiple resurrections are the norm, rather than the exception.

Rocking motion is strongly dependent on the characteristics of the timehistory waveform, regardless of whether one considers single pulses or entire records of ground motion [6–18]. Still, the pulse trains present in the latter make for a richer excitation, where minor details in the timing and amplitude of successive pulses can easily increase or decrease the response from one scaling level to another for the same waveform. This also holds for hysteretic systems, but it is of significantly lower magnitude thanks to the dampening effect of hysteresis. As Figure 1b shows, this is certainly not the case for rocking IDA curves, where extreme weaving behavior is often observed. This behavior persists throughout the entire range of response, from onset of rocking up to (and beyond) nominal overturning, the latter taken as the point where the peak rocking angle, θ_{max}, exceeds the block slenderness, a, for the first time. Thus, whenever this weaving pattern approaches the $\theta_{max} \approx a$ threshold (Figure 2), the rightmost parts of the weaves become collapses and the leftmost parts remain of stable response, creating a succession of overturning and non-overturning IM-levels. Sometimes these weaves are tight, leading to closely-spaced "dense" alternations of overturning and stable regions (Figure 2a), while in other cases they are broad, causing "sparse" resurrections separated by long continuous areas of instability (Figure 2b).

In general, the inclusion of resurrections into one's calculations will increase the maximum IM level that can still produce finite/stable EDP response, clearly affecting the resulting distributions. Thus, including them or not is a choice that is best left to the analyst. First of all, by nature, resurrections tend to appear at high IM and EDP levels. Thus, it is fundamental to understand the mechanics of the system involved and the fidelity of the idealized model at high response levels. At such large levels of IM and EDP, the islands of stability appearing after a resurrection are typically associated with fairly violent impacts and toe-crushing stresses that may be admissible for a small rigid block, but not for a sizeable structure or structural element of engineering significance. Then, for example, the simple rigid rocking block model may become unrealistic. Most systems of engineering significance (as well as their supporting base or foundation) will experience permanent toe or base deformation well before nominal overturning. In many ways, the mechanism of resurrection depends on the system remaining intact at high IM excitation. Neglecting such deterioration mechanisms is conducive to resurrections, but not necessarily physically realistic. Thus, one should ensure that the model can be trusted before embarking on further resurrection investigations.

In such cases, additional guidance may be offered by the damageability of the structure or component studied. For systems whose damage is associated solely with overturning, as is the case of non-fragile solid blocks, well-designed panel switches, etc., including resurrections may be a one-way street. In such cases, one should not terminate the IDA curves at the nominal overturning point, but instead employ an upper limit of a physically realizable IM, optimally informed by site-specific hazard information. On the contrary, systems that can sustain damage from rocking impact accelerations, such as museum artefacts, liquid-storage tanks, electromechanical equipment, or cloud servers, will only be negligibly affected by resurrections; the frequent damages produced by low IMs will tend to dominate any loss estimates in the same way that they do for most hysteretic structures. Then, stopping the IDAs at the appearance of first overturning should be adequate for all practical purposes.

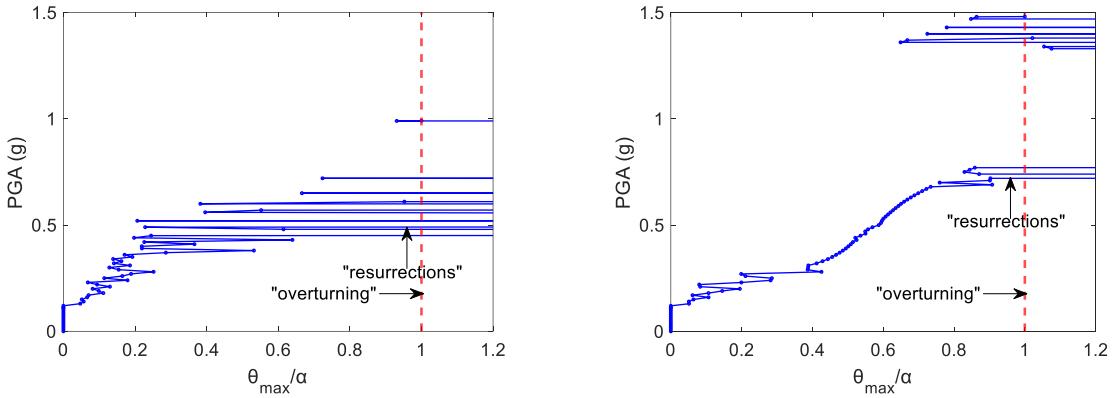

(a) "dense" nearby resurrections (b) "sparse" distanced resurrections

Figure 2. Typical IDA curves of a rocking block under single ground motions.

2.2 IDA functional inversion

An IDA curve, by nature and definition, is expressed as a function of the IM, $EDP = f(IM)$, since each nonlinear response history analysis run is performed at a given value of the IM and produces a single value of the EDP of interest. Although the $f(IM)$, or "given IM" form is sufficient for all practical purposes, an inverted "given EDP" form of $IM = f^{-1}(EDP)$ is advantageous for multiple applications that are characteristic of IDA. They all entail the characterization of the IM given EDP (IM|EDP) distribution [1] and can range from response-specific IM efficiency/sufficiency assessment [33] to the direct estimation of fragility curves [36]. Unfortunately, this inversion of the IDA curve is subject to the whims of weaving behavior. Figure 3a presents a typical example. On a given IM basis there is always one possible EDP value for each discrete value of the IM. On the other hand, for a given EDP underneath a weave, multiple possible IM values will appear along the vertical. Then, a mathematically correct definition of f^{-1} is not possible, as it should always return only a single IM output. What we instead seek is a convenient functional proxy that can serve the role of f^{-1}. This should closely follow the trends displayed by f, capturing the "average behavior" of the smoothened weaves, in turn producing IM|EDP distributions that match the results of EDP given IM (EDP|IM) ones in terms of fragility. To do so, one should choose where to optimally place this single IM output of f^{-1}. In terms of the example of Figure 3b, the range of such possible choices is any IM value between the first and the last of the three (or multiple in general) intersections. When the weavings are relatively rare, alike most hysteretic systems, this is a simple matter as all choices lead to practically identical results. Missing the "average behavior" for the few weavings here and there is inconsequential as it disappears in the ensemble statistics from multiple IDA curves. This led to the selection of the first (i.e., lowest) IM point appearing along the vertical, on the justification of seeking the first exceedance of a given EDP threshold, or the earliest appearance of the associated damage [1]. However, for the case of rocking blocks, the aforementioned frequent weaving behavior of the IDAs obviously complicates the inversion, as any bias in the process is replicated along nearly all ground motions and ends up severely impacting the resulting distributions.

Thus, a decision for the IM point that will be used for the inversion is needed. As Figure 3b shows, this choice is not trivial. The first/last-point techniques clearly bracket all other choices. They also produce by definition a monotone f^{-1}, which is a desirable mathematical property as it allows a reciprocal re-inversion of the proxy function, and a complete replacement of the initial IDA curve. Of course, both of these choices are clearly biased, as they produce extreme lows or extreme highs, misrepresenting the original f. For example, selecting the median (i.e. the second point in Figure 3a) or the mean of the intersection points (termed median/mean-point techniques, respectively) may offer an IDA curve that better matches the mid-point of all weaves; at the same time these techniques deliver some deviations from a desirable monotonicity. Whether any of these imperfect approaches will produce fragility-matching distributions is a question that remains to be answered.

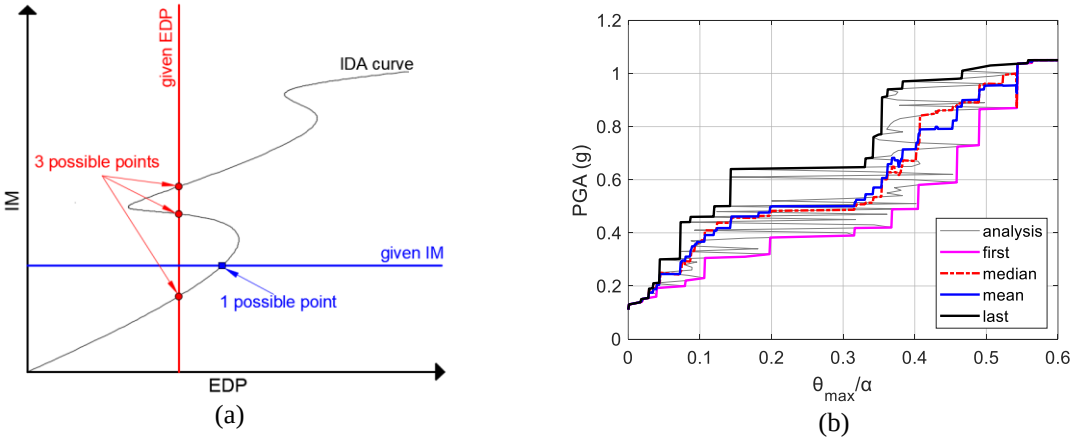

Figure 3. a) IM|EDP versus EDP|IM for a weaving rocking IDA curve, b) Different techniques for the inversion of the weaving IDA curve, comparing the first/median/mean/last-point choices.

2.3 Discretization and resolution

Statistics of IDA results (and in general of any random quantity) will depend on the number of the records (or samples) that is employed. Better, i.e., more efficient IMs [31–34] will, by definition, reduce the uncertainty in estimating response fractiles for a given system and number of records. Setting an acceptable level of uncertainty depends on the application at hand, with accurate assessment of the dispersion requiring more records relative to

the median or the mean. For example, Vamvatsikos and Cornell [2] have generally used 20 to 30 records for hysteretic systems, while Eads et. al [37] have argued that even using 274 records is not adequate to deliver robust results for the tails of the collapse fragility for a hysteretic structural system.

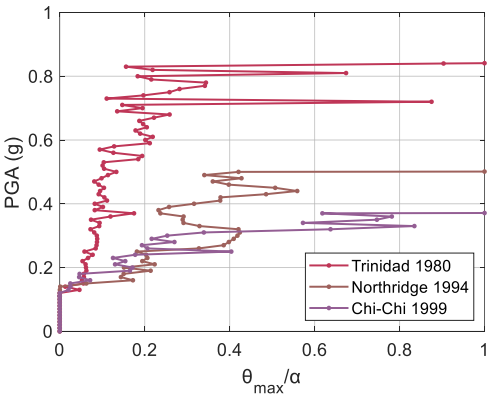

(a) 3 ordinary records

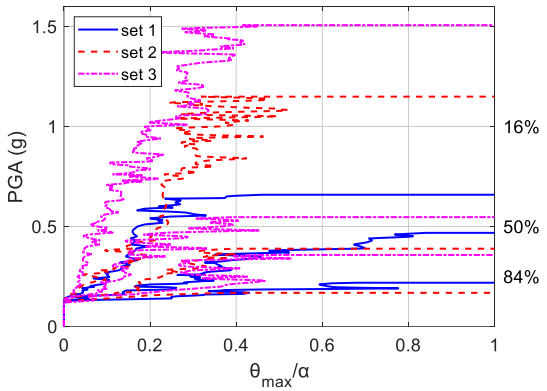

(b) 3 sets of 10 records

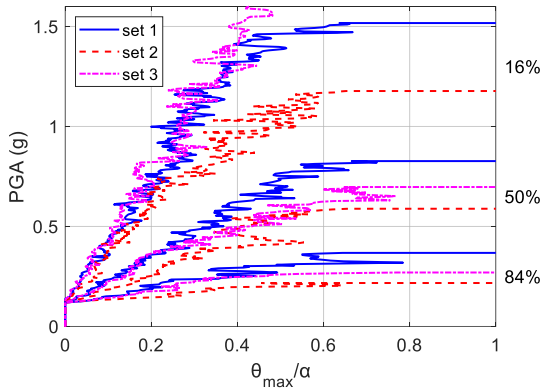

(c) 3 sets of 40 records

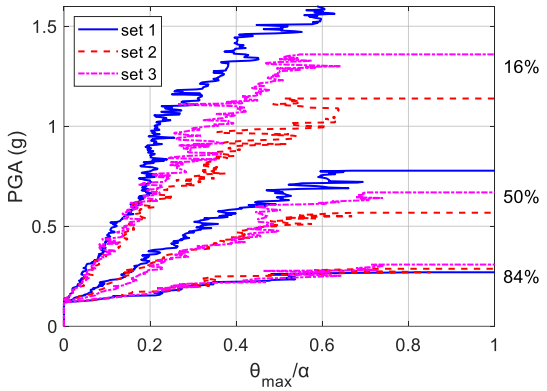

(d) 3 sets of 70 records

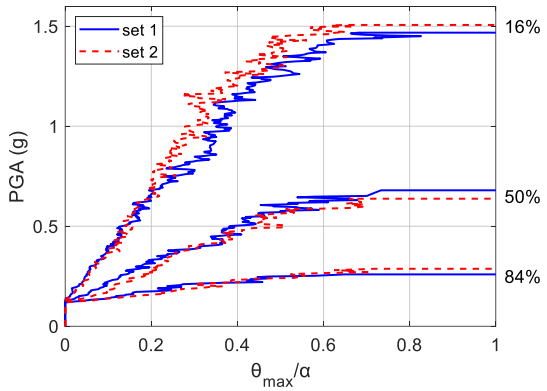

(e) 2 sets of 105 records

Figure 4. a) IDA curves for 3 ordinary records, versus 16/50/84% IDA EDP|IM fractiles for b) 3 sets of 10 ordinary records, c) 3 sets of 40 ordinary records, d) 3 sets of 80 ordinary records, e) 2 sets of 105 ordinary records.

For the case of a rocking block, the higher intrinsic record-to-record variability (Figure 4a) vis-à-vis hysteretic systems can only lead to the use of more ground motions to achieve similar levels of fidelity. Figures 4b-4e present the 16/50/84% EDP|IM quantiles for different sets of 10, 40, 70 and 105 ordinary ground motions, respectively. To ensure the fidelity of the investigation, different records have been employed in sets of the same size. Evidently, 10 records are a totally inefficient choice for the case of the rocking IDA leading to significant differences among sets both for the median as well as the dispersion. When increasing the number of records to 40 and above, differences in the median estimate between sets of the same size are significantly reduced. Actually, even different-size sets produce relatively similar median estimates. Still, the 84% and especially the 16% EDP|IM quantile do register non-negligible differences among sets of size 40 or 70 for relatively high EDP levels $(\tilde{\theta} > 0.40)$. Consequently, the dispersion will maintain some uncertainty in this region of response with such moderate sample

sizes. Finally, for the case of 105 records (Figure 4e), differences are all but eliminated for all the quantiles and the full range of response in the two sets sampled. Evidently, when investigating the rocking of a planar rigid body, 40–50 records seem to be a reasonable lower limit that can deliver an adequate level of accuracy for practical purposes. Still, the higher the number of the ground motions employed, the lower the dependence on individual IDA curves, and consequently the higher the fidelity of the results.

While having at least 40 records may resolve the issue of global bias by sufficiently stabilizing medians and dispersions, the weaving behavior of individual IDAs becomes another issue that can degrade the local fidelity of moderate-size record sets. Figure 4a, presents rocking IDAs for three different records, disregarding any resurrections. The highly weaving behavior is present in all cases. Contrarily, when looking at the summarized quantities (e.g., quantiles) of multiple records (Figure 4b-4e), residual weavings are smoothened down, with the increase in the number of records accelerating this effect. Large-scale weaves disappear first, however, even for the case of 105 records, some high frequency "noise" remains in the fractile estimates. One way to remove it is to employ a significantly higher number of records, e.g., of the order of 500 or 1000. However, this solution comes with obvious costs. Instead, the use of a monotone spline smoother [38, 39] is proposed as a more efficient way to sharpen the IDA fractiles without increasing the computational effort. Figure 5 illustrates the application of a monotone spline smoother to the median IDAs for one set of 40 records and another of 70 that also appear in Figures 4c and 4d, respectively. More aggressive smoothing can be employed for the set of 40, as large-scale weavings are present (Figure 5a). Less smoothing is required for the median of 70 records, since only some high frequency "noise" needs to be dampened out (Figure 5b). In the end, smoothing is not a panacea, as it will never make a smaller set equivalent to a larger one, but it will certainly improve the fidelity of both.

The number of the runs per record also affects the fidelity. More runs per record will lead to smaller steps that will obviously improve the resolution per IDA curve, mapping out weaves, discovering any resurrections, and bracketing islands of stability. At the same time, the number of runs is antagonistic to the number of records that can be employed for a given computational budget. Thus, one needs to find a balance between the two. Furthermore, arranging the selected budget of runs along an IDA curve is another non-negligible problem. Whereas the variable step hunt&fill algorithm [2] has obvious advantages for hysteretic systems, it may sometimes lead to large unexplored areas for rocking IDAs. Thus, a constant-size stepping scheme tends to be a simpler and better proposition. For example, to perfectly map out the IDAs in Figures 4–5, a constant step of 0.01 g is employed in terms of *PGA*. This allows the full investigation of the weaving behavior of individual rocking IDAs, while costing us 30–80 runs per each of the three records appearing in Figure 4a. Whether such level of detail is needed outside academic investigations is an interesting question, especially when weighed against the aforementioned needs to smoothen out weaves and employ large numbers of ground motions.

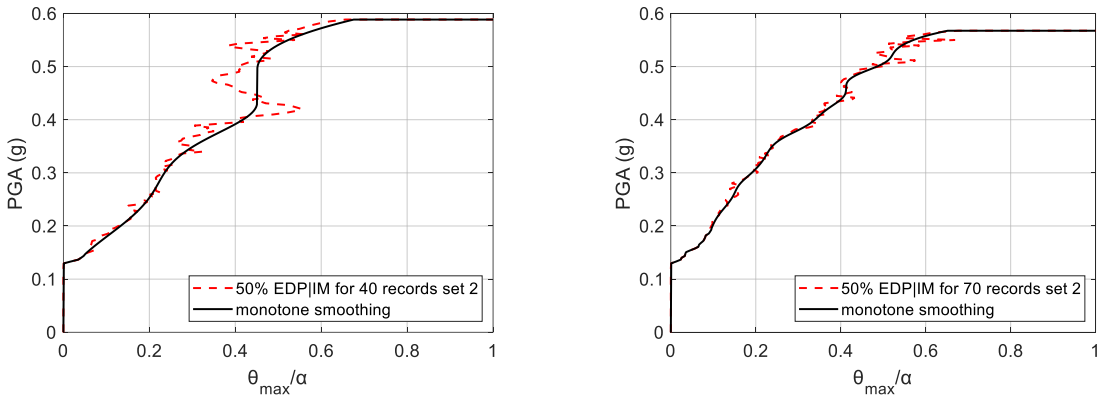

(a) 40 records (b) 70 records

Figure 5. Monotone smoothing of the 50% EDP|IM IDA fractile, for sets of (a) 40 ordinary records, and (b) 70 ordinary records.

3 CASE STUDIES AND INVESTIGATION OF OPTIONS

3.1 Blocks under investigation and analysis approach

To better illustrate the aforementioned issues, and the effect of analyst choices on the estimation of seismic response, three typical two-dimensional rectangular rigid rocking blocks are employed, indicated as C1 to C3. Table 1 illustrates their salient characteristics: Base width 2*b*, total height 2*h*, stability angle (also appearing in the

literature as slenderness) $a = \tan^{-1}(b/h)$, half diagonal $R = \sqrt{b^2 + h^2}$, frequency parameter $p = \sqrt{3g/(4R)}$, and the coefficient of restitution that represents the energy loss per impact during the rocking response, $n = 1 - (3/2)(\sin a)^2$ [6]. The three blocks represent simplified planar models of ancient monolithic columns of different slenderness. Of the three, column C2 resembles a semi-slender free-standing column of the Temple of Aphaia in Aegina, Greece. The dimensions of the other two columns have been selected to represent an arbitrary slender column (C1) and a semi-stocky one (C3).

Table 1. Block characteristics.

Block	2*b* (m)	2*h* (m)	*a* (rad)	*R* (m)	*p* (s^{-1})	*n*
C1	1.33	12.00	0.1104	6.04	1.1040	0.98
C2	0.95	5.29	0.1777	2.69	1.6546	0.95
C3	1.00	4.00	0.2450	2.06	1.8892	0.91

For the analysis, 105 ordinary no-long-duration, no-pulse-like, firm-soil ground motions were used; they were selected from the PEER database [40, 41] from events with moment magnitude of $M_w > 6.2$, having $PGA > 0.14$g. For the analysis, the scripts of Vassiliou [42] were employed. One horizontal component was arbitrarily-selected from each recording, employing its *PGA* as the IM, and the peak rocking angle normalized by slenderness of the block, $\tilde{\theta}$, as EDP. The former may not be the most efficient IM throughout the entire range of rocking response [e.g., 43, 44]; still, this makes little difference for the discussion that we intend to offer.

A constant step of 0.01 g was employed, starting from the first integer multiplier that exceeded the onset of rocking, i.e., $PGA \approx g \tan a$, and incrementing up to an upper limit of 3.50 g to explore the full rocking response, including at least one overturning point ($\tilde{\theta} \geq 1.00$) for nearly all (more than 95%) ground motions, plus any resurrections. Sliding was disregarded, assuming that the coefficient of friction is high enough to ensure pure planar rocking response. Figures 6a–c present the 105 IDA curves of the three columns, excluding all resurrections after the first (nominal) overturn for illustrative reasons. Highly weaving behavior and significant record-to-record variability are the norm. Actually, the latter is so high that a small number of records (fewer than 5%) fail to achieve overturning even for the extreme value of *PGA* = 3.50 g.

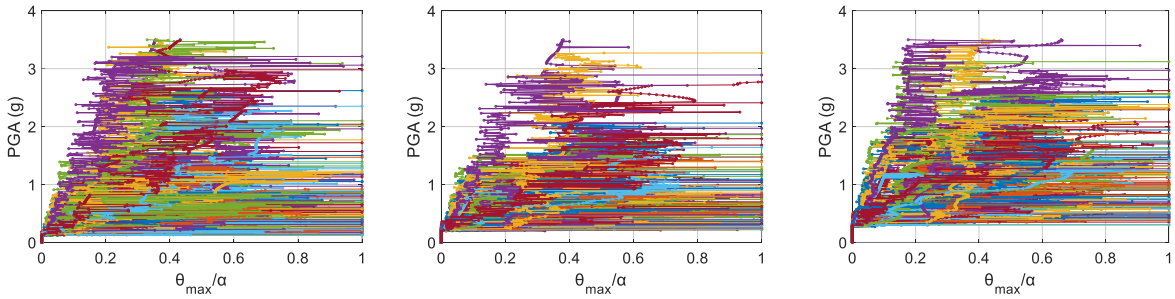

(a) C1 (b) C2 (c) C3

Figure 6. IDA curves for blocks C1–C3, without the inclusion of resurrections, still showing a wide range of weaving behaviors.

3.2 The effect of the inversion techniques

The IDA functional inversion techniques of first/last/mean/median point that were discussed in Section 2.2 are tested herein regarding the resulting statistical estimations. At this stage, the resurrections are disregarded, whereas their effect on the estimations is investigated in the next section. The comparison starts from the median IDA quantiles. Specifically, median IDAs that are calculated on the EDP|IM basis, requiring no inversion, are compared against the IM|EDP inverted basis results. Figure 7 shows the resulting median IDA for the three columns under investigation. As illustrated, the median and mean-point approaches produce IM|EDP medians that are close to the EDP|IM ones. On the other hand, taking the first/last-point path leads to notable differences and clearly biased median estimates. However, none of the inversion assumptions leads to inverted (IM|EDP) medians that perfectly match the given IM ones. To better assess the effect of the inversion techniques, a quantification of the relative bias for the different given EDP medians versus the standard of the given IM median is employed. First, a monotone smoother [38, 39] is applied to the comparison basis of the EDP|IM 50% curve, removing all weaves

and turning it into a one-to-one function; this can be readily inverted to produce a single value of PGA that corresponds to any given value of median $\tilde{\theta}$, denoted as $PGA\,|(\tilde{\theta}_{50\%} = \tilde{\theta})$ Note that, strictly speaking, this cannot be claimed to be the median $PGA|\tilde{\theta}$, but it certainly is what we would expect it to look like based on the expected correspondence of inverted IDA medians. Since it is this correspondence that we are trying to restore with our postprocessing, it makes sense to employ the smoothed $PGA\,|(\tilde{\theta}_{50\%} = \tilde{\theta})$ as our comparison basis. Then, for the j-th value of $\tilde{\theta}$ from the 1000 selected within [0,1], the relative bias for the i-th inversion technique is calculated as:

$$bias_{i,j} = \frac{PGA_{50\%}\,|\,\tilde{\theta}^j \text{ for technique } i}{PGA\,|(\tilde{\theta}_{50\%} = \tilde{\theta}^j) \text{ for the smoothed EDP|IM}} - 1 \quad (1)$$

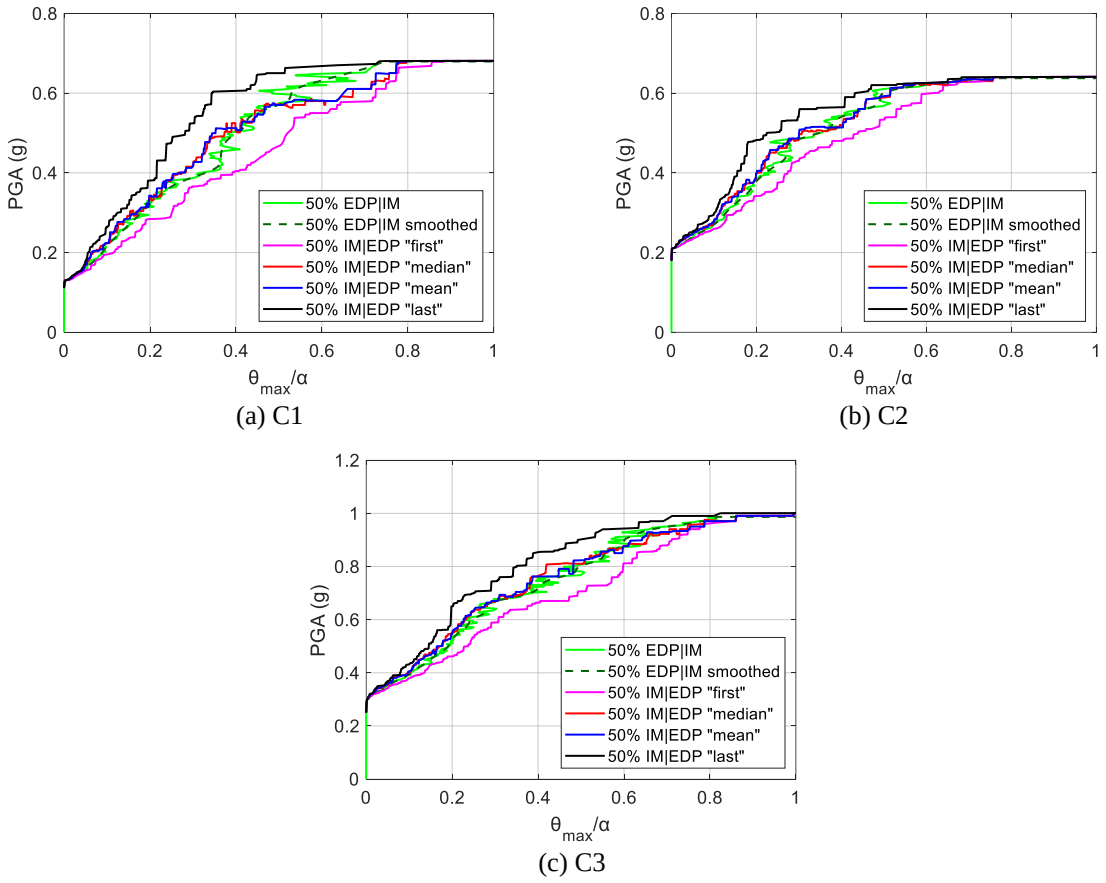

(a) C1 (b) C2

(c) C3

Figure 7. Median IDA curves estimated for 105 records via smoothed and raw EDP|IM results versus the four inversion techniques of first/median/mean/last point.

Figure 8 presents the bias in the median calculated via Eq. (1). As shown, the median/mean-point techniques produce similarly low bias, less than 0.10, for all the columns; the only exception appears for C1 at $\tilde{\theta} \approx 0.32 - 0.37$ where a spike reaching 0.20 is captured. This low bias makes these two techniques into fairly robust inversion tools, with the median-point assumption being considered slightly more reliable since is not affected by the inclusion of potentially extreme values. As expected, excessive relative bias is calculated for the first-point and especially for the last-point inversion techniques, with the latter sometimes exceeding 0.30 for C1 and C2. Note that, regardless of the inversion technique, any non-zero bias in Figure 8 is found for $\tilde{\theta} \approx 0.05 - 0.70$, at least when neglecting resurrections, as done herein. Naturally, for the model at hand, there is practically no bias for "deterministic" rocking initiation, at $PGA \approx g\tan\alpha$, or roughly $\tilde{\theta} < 0.05$. Similarly, near-zero bias is also captured for the near overturn area, or $\tilde{\theta} > 0.70$, since IDA curves reach their flatline at the first overturn occurrence (again when neglecting resurrections) and no weavings appear from this point on.

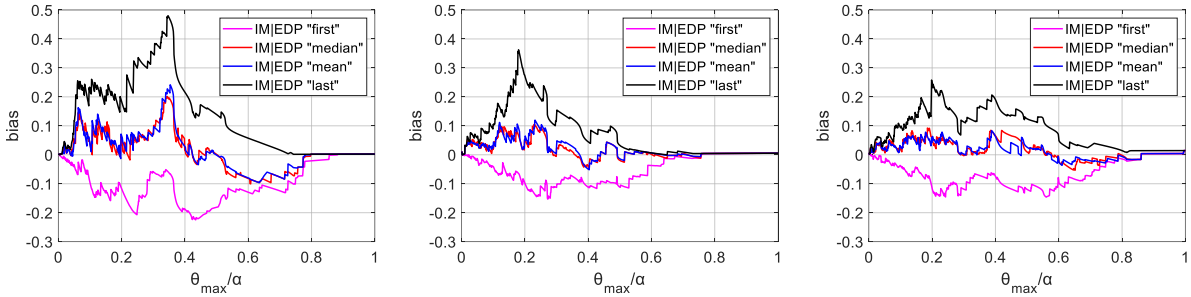

(a) C1 (b) C2 (c) C3

Figure 8. Bias per Eq. (1) of the median IM|EDP estimated for the three case study blocks via the four inversion techniques of first/median/mean/last point vis-à-vis the smoothed median EDP|IM.

Now the comparison turns into the record-to-record dispersion for the three columns. For the inverted IDA curves, dispersion is calculated as the standard deviation of the natural logarithm of the k = 1…105 values of $PGA^{k,j}$ (i.e., one per each of N = 105 records) estimated for each of j = 1…1000 $\tilde{\theta}^j$ points:

$$\beta_j = \sqrt{\frac{1}{N-1}\sum_{k=1}^{N}\left[\mu_{lnPGA}^{j} - \ln(PGA^{k,j})\right]^2} \tag{2}$$

where μ_{lnPGA}^{j} is the log-mean of 105 IM values corresponding to $\tilde{\theta}^j$. For the EDP|IM curves, the equivalent dispersion given the $\tilde{\theta}^j$ value can only be approximated from the smoothed EDP|IM 16% and 84% quantiles via a lognormal assumption, as smoothing is not implemented on individual IDA curves, only on summarized ones:

$$\beta_j' \approx \frac{1}{2}\left[\ln\left(PGA\,|(\tilde{\theta}_{16\%} = \tilde{\theta}^j)\right) - \ln\left(PGA\,|(\tilde{\theta}_{84\%} = \tilde{\theta}^j)\right)\right] \tag{3}$$

To even the scales, the same lognormal assumption approximation for the IM|EDP data would lead to an alternative of Eq. (2) that at least conforms to the basis as Eq. (3):

$$\beta_j \approx \frac{1}{2}\left[\ln\left(PGA_{84\%}\,|\tilde{\theta}^j\right) - \ln\left(PGA_{16\%}\,|\tilde{\theta}^j\right)\right] \tag{4}$$

Figure 9 compares the results of Eq. (2) and (3). First of all, the taller and lower-a block C1 has higher record-to-record dispersion vis-à-vis C2 and C3. This observation complies with the size-slenderness effects as they have been proposed by Housner [6] and investigated in detail by Makris and Kampas [45]. Still, in all cases dispersion is equal to zero at the initiation of rocking when PGA is employed as an IM due to the deterministic definition of the rocking initiation in terms of PGA. Then, in all cases a gradual increase follows until a final plateau of maximum dispersion is reached near overturning ($\tilde{\theta} > 0.70$). This is expected as PGA is efficient at the onset of rocking but becomes highly problematic close to overturning. Looking at the different inversion options, the median/mean-point techniques seem to better approximate the dispersion of the smoothed given-IM results. Some mismatches do appear, yet they are confined to relatively high dispersions where their magnitude can be considered acceptable. As expected, the first and last-point results bracket the mean/median-point ones, clearly introducing unneeded bias. These trends are also confirmed in Figure 10, which compares the estimates of Eq. (3) and (4), which are produced on an even basis of a lognormal assumption. Therein, even the small differences captured in Figure 9 for the mean/median-point curves tend to disappear, further supporting their validity.

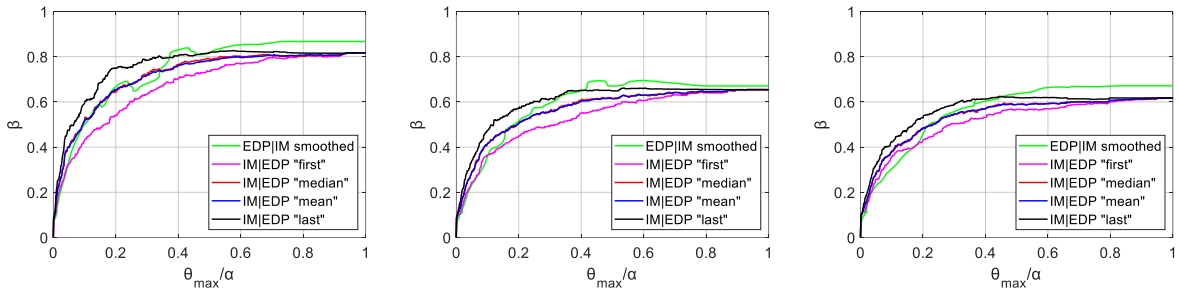

(a) C1 (b) C2 (c) C3

Figure 9. The dispersion from the smoothed 16/84% EDP|IM quantiles via Eq. (3) is compared against the dispersion of the IM|EDP IDAs per Eq. (2) via the inversion techniques of first/median/mean/last point.

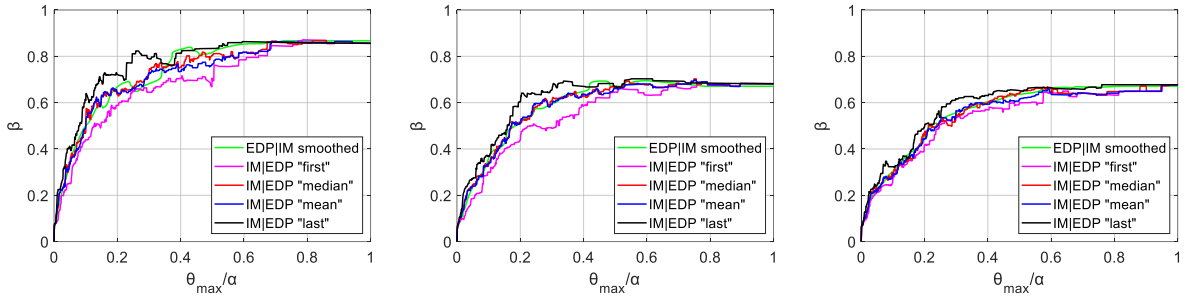

(a) C1 (b) C2 (c) C3

Figure 10. The dispersion from the smoothed 16/84% EDP|IM quantiles via Eq. (3) is compared against the dispersion of the IM|EDP IDAs per Eq. (4) for the inversion techniques of first/median/mean/last point.

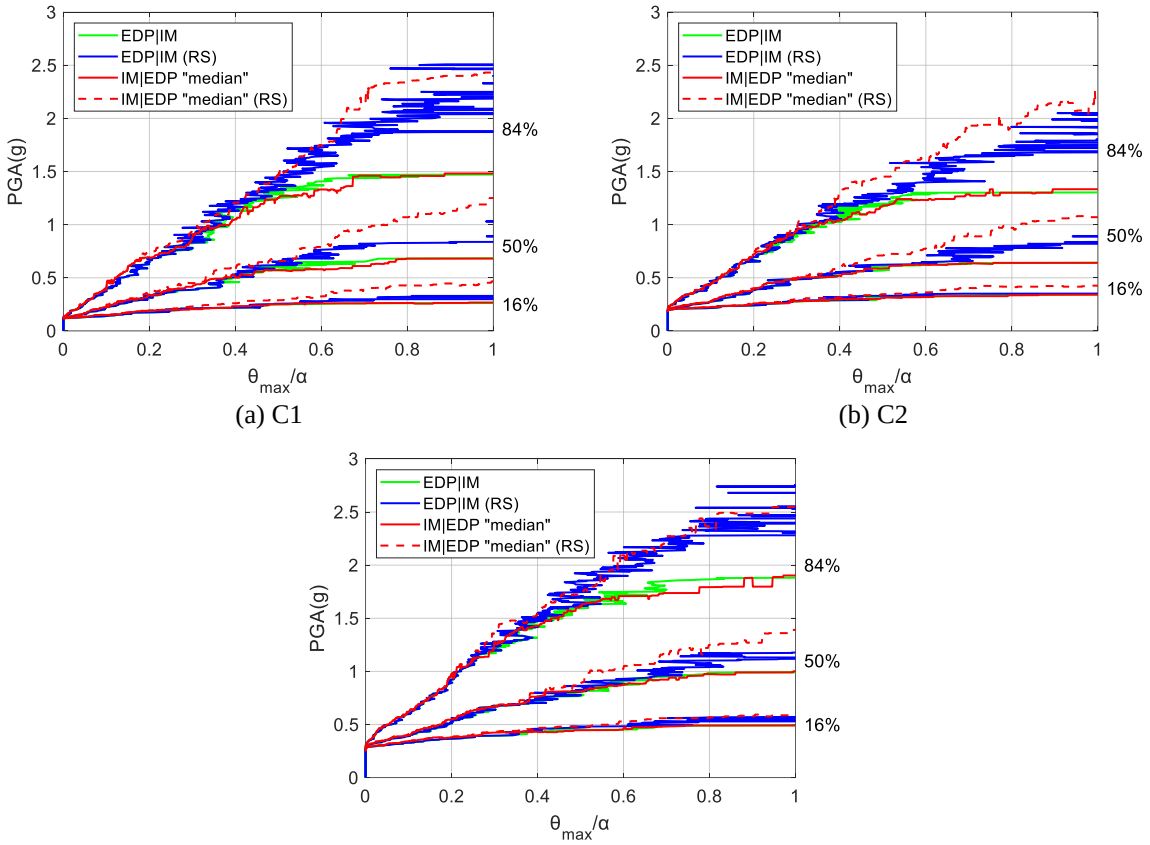

(a) C1 (b) C2

(c) C3

Figure 11. 16/50/84% IDA quantiles with resurrections (RS) versus without for 105 records and three columns. The influence is mainly isolated to the higher response and intensity levels. The 16% and 84% labels refer to the IM|EDP quantiles, which correspond to the 84% and 16% EDP|IM ones, respectively. The label 50% refers to the median quantiles of both the IM|EDP and EDP|IM cases.

3.3 The effect of resurrection points

As already discussed, the resurrections are a relatively frequent phenomenon for rocking blocks. Understanding the effect of including versus neglecting them on response distributions produced by IDA (or actually any other approach) is of interest. Figure 11 presents the 16/50/84% IDA quantiles for columns C1–C3, calculated with resurrections (denoted by "RS") versus without. Specifically, the EDP|IM as well as the median-point IM|EDP quantiles are provided. In all cases, only marginal differences are shown for $\tilde{\theta} < 0.60$ for the 16/50% IM|EDP quantiles, and $\tilde{\theta} < 0.40$ for the 84% IM|EDP quantiles. Contrarily, non-negligible differences are found for higher values of rocking response until the overturn ($\tilde{\theta} \approx 1.00$), especially for the 50% and 84% IM|EDP fractiles. These findings confirm our earlier observations on single record IDA, confining the influence of resurrections to the near-overturning area, where idealized models may become less reliable for structures and elements of engineering

significance. Thus, as discussed in Section 2.1 the inclusion of the resurrections into the analysis should be considered in tandem with the structure and model that are being investigated. Still, this only needs to be done when near-overturning responses are of interest. In all other cases, resurrections can safely be ignored without adverse consequences for the fidelity of the analysis.

Now, the comparison turns into the fragility functions as they are calculated with and without the inclusion of the resurrection points. For the fragility calculations both the horizontal and the vertical statistics methods [36] were employed. In general, the two methods yield near-identical fragility functions for the hysteretic structural systems [36]. Specifically, we calculate the probability $P(D > C|IM)$ of the seismic demand, D, exceeding the limit-state-specific EDP capacity threshold, C, given the IM value. For the EDP-basis approach (horizontal statistics) [36] the raw IDA curves were used, while for the IM-basis estimation (vertical statistics), the nearly-unbiased median-point and the relatively conservative first-point technique are employed. Of the two, the latter is unaffected from any resurrections, since it always captures the lowest point that is found along the vertical.

Figure 12 presents the empirical cumulative distribution functions (CDFs) defining the fragility for three different $\tilde{\theta}$ levels of block C1. For the low $\tilde{\theta} = 0.15$ threshold of Figure 12a, the fragilities are hardly affected by including/neglecting resurrections regardless of the method employed. Only the first-point technique leads to somewhat conservative results (i.e., shifted to the left), a trend that becomes intensified at higher $\tilde{\theta}$ thresholds, as expected. When going to $\tilde{\theta} = 0.50$ in Figure 12b, the effect of resurrections remains marginal for the EDP-basis approach (horizontal statistics) whereas it becomes noticeable on an IM-basis (vertical statistics), even when using the median-point technique. Still, differences up to this level of rocking response are generally low. Contrarily, for the overturning fragility function (Figure 12c), further differences appear. First of all, the overturning fragilities are identical for both the horizontal and vertical statistics when resurrections are neglected, since a single point at the unique flatline defines overturning. Including resurrections shifts the fragilities to the right, improving the estimated performance of the system; this fully conforms with our earlier observations about the influence of resurrections at high response levels.

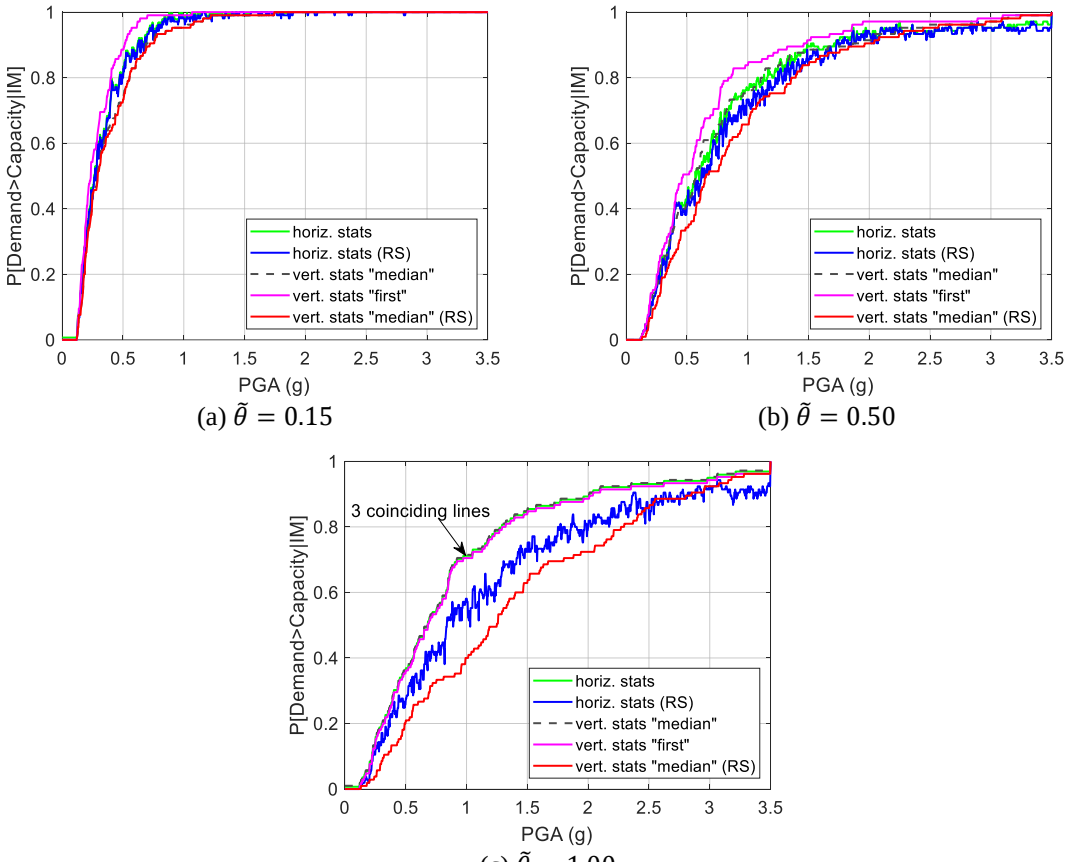

(a) $\tilde{\theta} = 0.15$ (b) $\tilde{\theta} = 0.50$

(c) $\tilde{\theta} = 1.00$

Figure 12. EDP-basis (horiz. stats) and IM-basis (vert. stats) empirical CDF fragility curves at predefined EDP capacity levels for block C1 from analysis with resurrections (RS) and without them for 105 ordinary records and three different response thresholds. A small shift has been introduced in (a) and (c) to visually separate coinciding curves.

Beyond just comparing the magnitude of different fragilities, Figure 12 offers information on their morphology as produced by each different method. First of all, the IM-basis estimates (vertical statistics) are always monotone functions by construction: They are empirical CDFs of the 105 discrete IM points (one point per record) corresponding to the given $\tilde{\theta}$ threshold. This monotonicity is a desirable attribute that is not present for horizontal statistics curves due to the high weaving behavior of the IDAs. Since these are not produced as a single function, but rather as an aggregation of $P(D > C|IM)$ values, one per IM level considered, they are vulnerable to the highly weaving nature of IDAs. Thus, high frequency "noise" appears, both when including and neglecting resurrections. The only exception is the case of the overturning fragility when resurrections are ignored, and there is no chance for a lower response to be registered at a higher IM for any IDA. Moreover, when using a smaller set of ground motions this "noise" is naturally amplified, as shown in Figures 13a–b for two EDP thresholds and 40 records. Restoring monotonicity by removing the high frequency "noise" makes sense, similarly to the case of the EDP|IM quantiles. It restores mathematical/theoretical consistency, while at the same time it reduces the need to run large record sets. To this end, a monotone spline smoother can be employed, similarly to Section 2.2. For instance, Figure 14 compares the three fragility functions for column C1 estimated via horizontal statistics against their smoothened versions; the latter are clearly closer to what we would expect a fragility to look like.

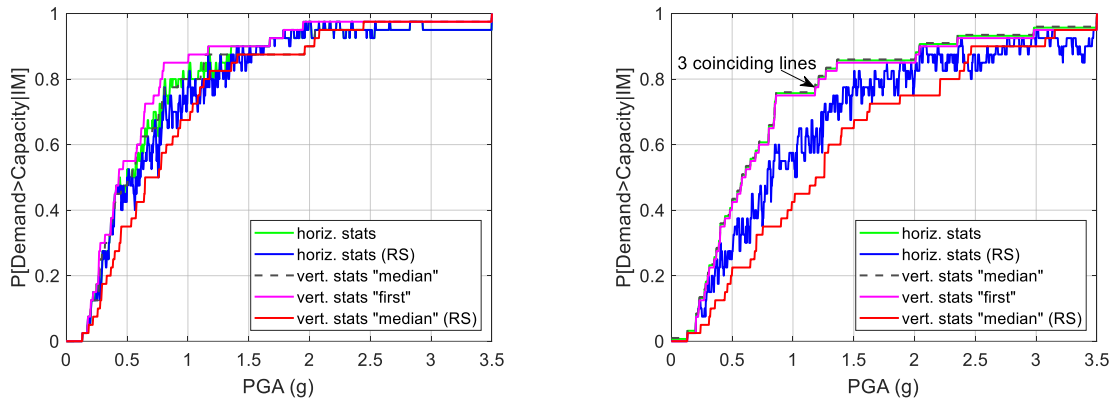

(a) $\tilde{\theta} = 0.50$ (b) $\tilde{\theta} = 1.00$

Figure 13. EDP-basis (horiz. stats) and IM-basis (vert. stats) empirical CDF fragility curves for block C1 including resurrections (RS) versus neglecting them for 40 ordinary records and two EDP thresholds: a) $\tilde{\theta} = 0.50$, b) $\tilde{\theta} = 1.00$, A small shift has been introduced in (b) to visually separate coinciding curves.

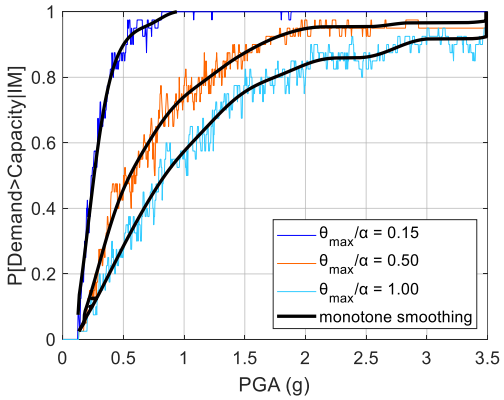

Figure 14. EDP-basis (horiz. stats) empirical CDF fragility curves for block C1 including resurrections for 40 ordinary records and three EDP thresholds: Raw "noisy" curves versus smoothened ones.

3.4 The effect of the number of runs per record

For all analyses shown so far, a computationally-expensive high-resolution approach has been employed utilizing a constant step of 0.01 g that can easily lead to hundreds of runs per record, even if one only wants to reach the first overturning IM. This was a conscious decision to ensure the fidelity of the results by capturing "all" weavings and block resurrections. Such a detailed study is not essential for practical purposes, which begs the question of

how far one can relax the fidelity requirements (i.e., increase the step size) to save on the number of analyses. For the comparison, the full initial analysis up to PGA = 3.50 g at a 0.01 g step is used as a benchmark, gradually removing runs to produce sets corresponding to constant steps of 0.02 g, 0.03 g, 0.05 g and 0.10 g. To ensure that at least one non-overturning point is always included in the results, removal of runs was initiated after the first rocking response point, i.e., the one that is closest to $PGA \approx g \tan\alpha$. For both the initial and the new sets, all results above the first overturning point were discarded, wherever this was encountered in the simulated analysis series. In other words, coarser runs easily missed low-IM overturning points, resulting to artificially high estimates of the first occurrence of overturning.

Figure 15 compares the results of the different step-size strategies for the example of block C2. Figure 15a captures the given IM medians, whereas Figures 15b and 15c the given EDP ones, for the median and first-point techniques, respectively. Larger steps tend to push the median to higher IM levels, a trend that is noticeable mainly close to overturning $\tilde{\theta} > 0.60$ for the 0.05 g and 0.10 g step cases, with the results being marginally worse for the first-point technique. This overall trend is consistent to missing some lower overturning points when using larger steps, thus inflating the median estimate. However, no excessive differences are present in any example. This is further confirmed for the given EDP dispersion, β, as calculated via Eq. (2) for the median-point technique in Figure 15d. The results are near identical for all step sizes up to 0.05 g, whereas somewhat higher dispersion is captured for the 0.10 g step for $\tilde{\theta} > 0.40$. Consequently, steps up to 0.05 g or even up to 0.10 g seem to be efficient alternatives for practical purposes when a large record set is employed. Larger steps are not recommended, at least for the simple rocking blocks investigated, due the high nonlinearity of the rocking response in association with the strong dependence on the waveform of the ground motion that may lead to deficient IDAs.

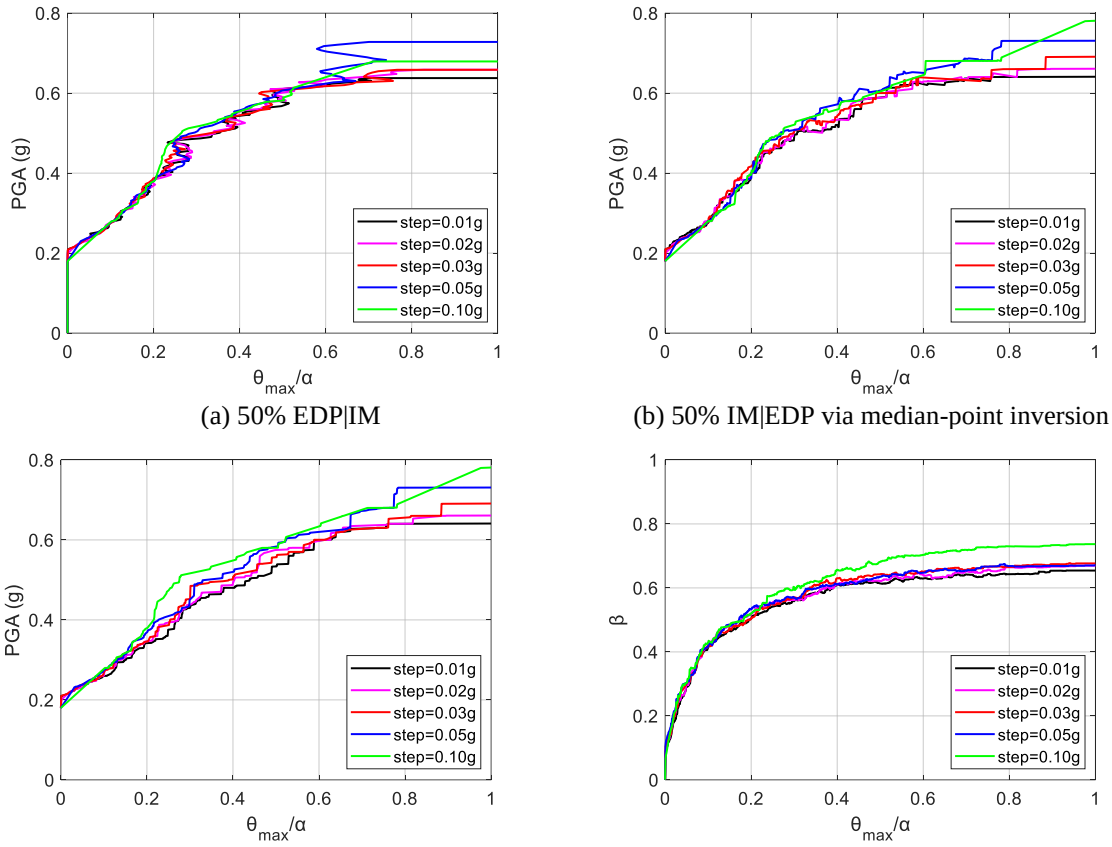

(a) 50% EDP|IM

(b) 50% IM|EDP via median-point inversion

(c) 50% IM|EDP via first-point inversion

(d) dispersion via Eq. (2) for the median-point inverted IDA curves

Figure 15. The effect of step size (or number of runs per record) for block C2, shown for the median EDP|IM and IM|EDP curves, as well as the given-EDP dispersions. In all cases, the differences are low enough to support the use of larger steps when determining response distributions and fragilities.

4 CONCLUSIONS

Incremental Dynamic Analysis is a valid approach for evaluating the seismic response of rigid rocking blocks. Its application, though, needs to account for the unconventional nature of rocking response, displaying multiple resurrection points and heavily weaving behaviors that defy intuition gained from hysteretic systems.

- When encountering resurrections, including or neglecting them is a choice that should be made in consideration of the application, the system and the model employed. Still, this only affects near-overturning response, allowing us to discard resurrections when losses appear at lower levels of response.
- Inverting IDA curves to recover quantiles of intensity given a level of response (as it pertains to the estimation of fragilities), is not a well-defined operation as multiple corresponding intensity values are frequently encountered. Selecting the median value is a nearly unbiased strategy that closely matches the quantiles of response given intensity.
- Smoothing, e.g., via a monotone spline smoother is a useful approach to remove residual "noise" from weaving that would otherwise degrade the quality of quantile results and fragility estimates produced from moderate-size record sets. This allows the use of fewer records with low consequences.
- Increasing the step size (and reducing the number of runs per record) can be done within reason, especially if a large number of records is employed to reduce the effect of missing low intensity overturning points.

While only planar rigid blocks undergoing pure rocking have been investigated, the findings are applicable to any structural system with highly weaving, highly variable behavior, offering a blueprint for applications well beyond the narrow range of the examples presented.

ACKNOWLEDGEMENTS

This research has been co-financed by the European Regional Development Fund of the European Union and Greek national funds through the Operational Program Competitiveness, Entrepreneurship and Innovation, under the call RESEARCH – CREATE – INNOVATE (project code: T1EDK-00956), project: "ARCHYTAS: Archetypal telemetry and decision support system for the protection of monumental structures". Financial support has been also provided by the "HYPERION–Development of a decision support system for improved resilience & sustainable reconstruction of historic areas to cope with climate change & extreme events based on novel sensors and modelling tools", Grant Agreement number 821054. The authors would like to thank Drs E.G. Dimitrakopoulos and M.F. Vassiliou for providing comments and constructive suggestions for improving this research work. Dr Vassiliou is also acknowledged for providing the software for undertaking the numerical study on the rocking oscillators under earthquake excitations.

DATA AVAILABILITY STATEMENT

The data that support the findings of this study are available from the corresponding author upon reasonable request.

CONFLICT OF INTEREST STATEMENT

The authors declare that they have no conflicts of interest.

REFERENCES

[1] Vamvatsikos D, Cornell CA. Incremental dynamic analysis. *Earthquake Engineering and Structural Dynamics*, 2002;**31**(3):491–514. https://doi.org/10.1002/eqe.141

[2] Vamvatsikos D, Cornell CA. Applied incremental dynamic analysis. *Earthquake Spectra*, 2004;**20**(2):523–553. https://doi.org/10.1193/1.1737737

[3] Marriott D, Pampanin S, Palermo A. Quasi-static and pseudo-dynamic testing of unbonded post-tensioned rocking bridge piers with external replaceable dissipaters. *Earthquake Engineering and Structural Dynamics*, 2009;**38**(3):331–354. https://doi.org/10.1002/eqe.857

[4] Kurama Y, Pessiki S, Sause R, Lu LW. Seismic behavior and design of unbonded post-tensioned precast concrete Walls. *PCI Journal*, 1999;**44**(3):72–89. https://doi.org/10.15554/pcij.05011999.72.89

[5] Bachmann JA, Vassiliou MF, Stojadinović B. Dynamics of rocking podium structures. *Earthquake Engineering and Structural Dynamics*, 2017;**46**(14): 2499–2517. https://doi.org/10.1002/eqe.2915

[6] Housner GW. The behavior of inverted pendulum structures during earthquakes. *Bulletin of the Seismological Society of America*, 1963;**53**(2):403–417.

[7] Yim C-S, Chopra AK, Penzien J. Rocking response of rigid blocks to earthquakes. *Earthquake Engineering and Structural Dynamics*, 1980;**8**(6):565–587. https://doi.org/10.1002/eqe.4290080606

[8] Ishiyama Y. Motions of rigid bodies and criteria for overturning by earthquake excitations. *Earthquake Engineering and Structural Dynamics*, 1982;**10**(5):635–650. https://doi.org/10.1002/eqe.4290100502

[9] Spanos PD, Koh AS. Rocking of Rigid blocks due to harmonic shaking. *Journal of Engineering Mechanics (ASCE)*, 1984;**110**(11):1627–1642. https://doi.org/10.1061/(ASCE)0733-9399(1984)110:11(1627)

[10] Makris N, Roussos Y. Rocking response of rigid blocks under near-source ground motions. *Géotechnique*, 2000;**50**(3):243–262. https://doi.org/10.1680/geot.2000.50.3.243

[11] Zhang J, Makris N. Rocking response of free-standing blocks under cycloidal pulses. *Journal of Engineering Mechanics (ASCE)*, 2001;**127**(5):473–483. https://doi.org/10.1061/(ASCE)0733-9399(2001)127:5(473)

[12] Makris N, Konstantinidis D. The rocking spectrum and the limitations of practical design methodologies. *Earthquake Engineering and Structural Dynamics*, 2003;**32**(2):265–289. https://doi.org/10.1002/eqe.223

[13] Vassiliou MF, Makris N. Analysis of the rocking response of rigid blocks standing free on a seismically isolated base. *Earthquake Engineering and Structural Dynamics*, 2012;**41**(2):177–196. https://doi.org/10.1002/eqe.1124

[14] Dimitrakopoulos EG, DeJong MJ. Revisiting the rocking block: closed-form solutions and similarity laws. *Proceedings of the Royal Society A: Mathematical, Physical and Engineering Sciences*, 2012;**468**(2144):2294–2318. https://doi.org/10.1098/rspa.2012.0026

[15] Makris N, Vassiliou MF. Planar rocking response and stability analysis of an array of free-standing columns capped with a freely supported rigid beam. *Earthquake Engineering and Structural Dynamics*, 2013;**42**(3):431–449. https://doi.org/10.1002/eqe.2222

[16] Voyagaki E, Psycharis IN, Mylonakis G. Rocking response and overturning criteria for free standing rigid blocks to single-lobe pulses. *Soil Dynamics and Earthquake Engineering*, 2013;**46**:85–95. https://doi.org/10.1016/j.soildyn.2012.11.010

[17] Dimitrakopoulos EG, Paraskeva TS. Dimensionless fragility curves for rocking response to near-fault excitations. *Earthquake Engineering and Structural Dynamics*, 2015;**44**(12):2015–2033. https://doi.org/10.1002/eqe.2571

[18] Bachmann JA, Strand M, Vassiliou MF, Broccardo M, Stojadinović B. Is rocking motion predictable? *Earthquake Engineering and Structural Dynamics*, 2018;**47**(2):535–552. https://doi.org/10.1002/eqe.2978

[19] Konstantinidis, D, Makris, N. Experimental and analytical studies on the response of freestanding laboratory equipment to earthquake shaking. *Earthquake Engineering and Structural Dynamics*, 2009;**38**(6):827–848. https://doi.org/10.1002/eqe.871

[20] Fragiadakis M, Diamantopoulos S. Fragility and risk assessment of freestanding building contents. *Earthquake Engineering and Structural Dynamics*, 2020;**49**(10):1028–1048. https://doi.org/10.1002/eqe.3276

[21] Berto L, Meroi E, Rocca I, Saetta A. Rocking activation of free standing elements in real conditions: A safe experimentally-based acceleration limit. *Engineering Structures*, 2021;**226**:111331. https://doi.org/10.1016/j.engstruct.2020.111331

[22] FEMA. *Quantification of Building Seismic Performance Factors*. FEMA P-695, prepared by Applied Technology Council for Federal Emergency Management Agency, Washington, D.C. 2009.

[23] FEMA. *Seismic Performance Assessment of Buildings*. FEMA P-58, prepared by the Applied Technology Council for the Federal Emergency Management Agency, Washington, D.C. 2012.

[24] D'Ayala D, Meslem A, Vamvatsikos D, Porter K, Rossetto T, Silva V. *Guidelines for analytical vulnerability assessment of low/mid-rise buildings – Methodology*. Pavia, Italy: Vulnerability Global Component Project. 2015.

[25] Jalayer F, Cornell CA. Alternative non-linear demand estimation methods for probability-based seismic assessments. *Earthquake Engineering and Structural Dynamics*, 2009;**38**(8):951–972. https://doi.org/10.1002/eqe.876

[26] Cornell CA, Jalayer F, Hamburger RO, Foutch DA. Probabilistic basis for 2000 SAC federal emergency management agency steel moment frame guidelines. *Journal of Structural Engineering (ASCE)*, 2002;**128**(4):526–533. https://doi.org/10.1061/(ASCE)0733-9445(2002)128:4(526)

[27] Baker JW, Cornell CA. Spectral shape, epsilon and record selection. *Earthquake Engineering and Structural Dynamics*, 2006;**35**(9):1077–1095. https://doi.org/10.1002/eqe.571

[28] Bradley BA. A generalized conditional intensity measure approach and holistic ground-motion selection. *Earthquake Engineering and Structural Dynamics*, 2010;**39**(12):1321–1342. https://doi.org/10.1002/eqe.995

[29] Kohrangi M, Bazzurro P, Vamvatsikos D, Spillatura A. Conditional spectrum-based ground motion record selection using average spectral acceleration *Earthquake Engineering and Structural Dynamics*, 2017; **46**(10):1667–1685. https://doi.org/10.1002/eqe.2876

[30] Kohrangi M, Vamvatsikos D, Bazzurro P. Multi-level conditional spectrum-based record selection for IDA. *Earthquake Spectra*, 2020;**36**(4):1976–1994. https://doi.org/10.1177/8755293020919425

[31] Vamvatsikos D, Cornell C.A. Developing efficient scalar and vector intensity measures for IDA capacity estimation by incorporating elastic spectral shape information. *Earthquake Engineering and Structural Dynamics*, 2005;**34**(13):1573–1600. https://doi.org/10.1002/eqe.496

[32] Luco N, Cornell CA. Structure-Specific scalar intensity measures for near-source and ordinary earthquake ground motions. *Earthquake Spectra*, 2007;**23**(2):357–392. https://doi.org/10.1193/1.2723158

[33] Kazantzi AK, Vamvatsikos D. Intensity measure selection for vulnerability studies of building classes. *Earthquake Engineering & Structural Dynamics*, 2015;**44**(15):2677–2694. https://doi.org/10.1002/eqe.2603

[34] Eads L, Miranda E, Lignos DG. Average spectral acceleration as an intensity measure for collapse risk assessment. *Earthquake Engineering and Structural Dynamics*, 2015;**44**(12):2057–2073. https://doi.org/10.1002/eqe.2575

[35] Psycharis IN, Papastamatiou DY, Alexandris AP. Parametric investigation of the stability of classical columns under harmonic and earthquake excitations. *Earthquake Engineering and Structural Dynamics*, 2000;**29**(8):1093–1109. https://doi.org/10.1002/1096-9845(200008)29:8<1093::AID-EQE953>3.0.CO;2-S

[36] Bakalis K, Vamvatsikos D. Seismic fragility functions via nonlinear response history analysis. *Journal of Structural Engineering (ASCE)*, 2018;144(10):04018181. https://doi.org/10.1061/(ASCE)ST.1943-541X.0002141

[37] Eads L, Miranda E, Krawinkler H, Lignos DG. An efficient method for estimating the collapse risk of structures in seismic regions. *Earthquake Engineering and Structural Dynamics*, 2013;**42**(1):25–41. https://doi.org/10.1002/eqe.2191

[38] Ramsay JO. Estimating smooth monotone functions, *Journal of the Royal Statistical Society: Series B (Statistical Methodology)*, 1998;**60**(2):365–375. https://doi.org/10.1111/1467-9868.00130

[39] Zhang J-T. A simple and efficient monotone smoother using smoothing splines, *Journal of Nonparametric Statistics*, 2004;**16**(5):779–796. https://doi.org/10.1080/10485250410001681167

[40] PEER NGA Database. Pacific Earthquake Engineering Research Center, Berkeley, CA, 2005 http://peer.berkeley.edu/nga/ (Jul. 27, 2021).

[41] Chiou B, Darragh R, Gregor N, Silva W. NGA Project Strong-Motion Database. *Earthquake Spectra*, 2008;**24**(1):23–44. http://dx.doi.org/10.1193/1.2894831

[42] Vassiliou MF. Rocking response of a rigid block to a ground motion, MATLAB script: available at https://n.ethz.ch/~mvassili/scripts.html last accessed October 2021.

[43] Makris N, Black CJ. Evaluation of peak ground velocity as a 'good' intensity measure for near-source ground motions. *Journal of Engineering Mechanics* (ASCE), 2004;**130**(9):1032–1044. https://doi.org/10.1061/(ASCE)0733-9399(2004)130:9(1032)

[44] Giouvanidis AI, Dimitrakopoulos EG. Rocking amplification and strong-motion duration. *Earthquake Engineering and Structural Dynamics*, 2018;**47**(10):2094–2116. https://doi.org/10.1002/eqe.3058

[45] Makris N, Kampas G. Size versus slenderness: two competing parameters in the seismic stability of free-standing rocking columns. *Bulletin of the Seismological Society of America*, 2016;**106**(1):104. http://dx.doi.org/10.1785/0120150138